Published OnlineFirst August 29, 2017; DOI: 10.1158/1078-0432.CCR-17-0647

Cancer Therapy: Preclinical

Clinical Cancer Research

Macrophages Facilitate Resistance to Anti-VEGF Therapy by Altered VEGFR Expression

Heather J. Dalton[1], Sunila Pradeep[1,2], Michael McGuire[1], Yared Hailemichael[3], Shaolin MA[1], Yasmin Lyons[1], Guillermo N. Armaiz-Pena[1], Rebecca A. Previs[1], Jean Marie Hansen[1], Rajesha Rupaimoole[1], Vianey Gonzalez-Villasana[4,5], Min Soon Cho[6], Sherry Y. Wu[1], Lingegowda S. Mangala[1,7], Nicholas B. Jennings[1], Wei Hu[1], Robert Langley[8], Hong Mu[9], Michael Andreeff[9], Menashe Bar-Eli[8], Willem Overwijk[3], Prahlad Ram[10], Gabriel Lopez-Berestein[4,7], Robert L. Coleman[1], and Anil K. Sood[1,7,8]

Abstract

Purpose: VEGF-targeted therapies have modest efficacy in cancer patients, but acquired resistance is common. The mechanisms underlying such resistance are poorly understood.

Experimental Design: To evaluate the potential role of immune cells in the development of resistance to VEGF blockade, we first established a preclinical model of adaptive resistance to anti-VEGF therapy. Additional *in vitro* and *in vivo* studies were carried out to characterize the role of macrophages in such resistance.

Results: Using murine cancer models of adaptive resistance to anti-VEGF antibody (AVA), we found a previously unrecognized role of macrophages in such resistance. Macrophages were actively recruited to the tumor microenvironment and were responsible for the emergence of AVA resistance. Depletion of macrophages following emergence of resistance halted tumor growth and prolonged survival of tumor-bearing mice. In a macrophage-deficient mouse model, resistance to AVA failed to develop, but could be induced by injection of macrophages. Downregulation of macrophage VEGFR-1 and VEGFR-3 expression accompanied upregulation of alternative angiogenic pathways, facilitating escape from anti-VEGF therapy.

Conclusions: These findings provide a new understanding of the mechanisms underlying the modest efficacy of current anti-angiogenesis therapies and identify new opportunities for combination approaches for ovarian and other cancers. *Clin Cancer Res; 23(22); 7034–46. ©2017 AACR.*

Introduction

Angiogenesis is a hallmark of cancer and is essential for tumor growth and metastasis (1). Of the complex mechanisms regulating blood vessel formation in cancer, the VEGF family and associated receptors are recognized as a dominant pathway (2). VEGF (VEGF-A) exerts its effects largely through VEGF receptor (VEGFR)-2 and acts as the central promoter of tumor angiogenesis (3). As VEGF is constitutively overexpressed in many cancers, therapies targeting this pathway were highly anticipated additions to standard chemotherapeutic drugs (4). Yet, clinical survival benefits from antiangiogenic therapies have been modest (5); resistance to these agents often emerges, and tumor growth resumes, along with rapid revascularization following termination of these therapies (6, 7). Indeed, several clinical trials show the collapse of survival curves and clinical benefit following cessation of therapy with antiangiogenic agents such as bevacizumab (8–10). The mechanisms responsible for these clinical phenomena remain unclear; however, possible avenues for escape from VEGF blockade lie in the stromal components of the tumor microenvironment.

Populations of macrophages express Tie2 and are capable of vascular mimicry through the expression of endothelial cell markers and the formation of capillary-like structures in response to VEGF, possibly paving the way for vessel maturation with replacement by true endothelial cells (11). It is already reported that inherent anti-VEGF refractoriness is associated with infiltration of the tumor tissue by $CD11b^{+}Gr1^{+}$ myeloid cells (12). Furthermore, macrophages have been implicated in the development of resistance to antitumor therapies, including platinum-based chemotherapy and

[1]Departments of Gynecologic Oncology and Reproductive Medicine, [2]Department of Obstetrics and Gynecology, Medical College of Wisconsin, Milwaukee, WI, 53226, USA. [3]Department of Melanoma Medical Oncology, [4]Experimental Therapeutics, [5]Departamento de Biologia Celular y Genetica, Universidad Autonoma de Nuevo Leon, San Nicolas de los Garza, Nuevo Leon, Mexico. [6]Benign Hematology, The University of Texas MD Anderson Cancer Center, Houston, Texas. [7]Center for RNA Interference and Non-Coding RNAs, The University of Texas MD Anderson Cancer Center, Houston, Texas. [8]Cancer Biology, The University of Texas MD Anderson Cancer Center, Houston, Texas. [9]Section of Molecular Hematology and Therapy, Department of Leukemia, The University of Texas MD Anderson Cancer Center, Houston, Texas. [10]Department of Systems Biology, The University of Texas MD Anderson Cancer Center, Houston, Texas.

Note: Supplementary data for this article are available at Clinical Cancer Research Online (http://clincancerres.aacrjournals.org/).

H.J. Dalton and S. Pradeep equally contributed to this article.

Corresponding Author: A.K. Sood, The University of Texas MD Anderson Cancer Center, 1515 Holcombe Blvd., Unit 1362, Houston, TX 77030. Phone: 713-745-5266; Fax: 713-792-7586; E-mail: asood@mdanderson.org

doi: 10.1158/1078-0432.CCR-17-0647

Published OnlineFirst August 29, 2017; DOI: 10.1158/1078-0432.CCR-17-0647

Translational Relevance

Although anti-VEGF antibody has provided clinical benefit for cancer patients, adaptive resistance develops rapidly in most, limiting its utility. We found that macrophages in the tumor microenvironment orchestrate anti-VEGF therapy resistance. At the emergence of resistance, depletion of macrophage VEGFR-1 and VEGFR-3 expression accompanies upregulation of alternative angiogenic pathways, facilitating escape from anti-VEGF therapy. Macrophage depletion could be used to improve the effectiveness of VEGF blockade in the treatment of cancer patients. These findings have significant implications for clinical management of cancer patients.

radiotherapy (13–15). Through their ability to induce proangiogenic pathways, macrophages may play important roles in resistance to drugs targeting the VEGF/VEGFR pathways (16).

To identify potential mechanisms of adaptive resistance to anti-VEGF therapy, we carried out a series of *in vitro* and *in vivo* experiments and found that macrophages actively contribute to resistance to anti-VEGF therapy. Importantly, we demonstrate a previously unrecognized ability of macrophages to adapt to anti-VEGF therapies through modulation of VEGFR expression and other proangiogenic factors.

Materials and Methods

Cell lines and tissue culture

IG10 cells were maintained in DMEM supplemented with 5% FBS, 1x insulin-transferrin-sodium selenite supplement (Roche Diagnostics), and 0.1% gentamicin sulfate (Gemini Bio Products). OVCAR5 cells were maintained in DMEM with 10% FBS and 0.1% gentamicin sulfate. SKOV3ip1 cells were maintained in RPMI 1640 medium supplemented with 15% FBS and 0.1% gentamicin sulfate. All cell lines were validated by short tandem repeat fingerprinting and were routinely screened for mycoplasma. Experiments were performed at 60% to 80% cell confluence.

Immortomouse macrophages

Immortomouse macrophages, a kind gift from Dr. Robert Langley, were maintained in DMEM with 10% FBS and 0.1% gentamicin sulfate. These conditionally immortalized cells are derived from the Immortomouse (The Jackson Laboratory) and bear a transgene that allows interferon-inducible expression of a thermolabile large tumor antigen (and the small tumor antigen) from the SV40 thermosensitive A58 strain directed to widespread tissues by the IFN-inducible Class I antigen promoter from the mouse H-2Kb locus. The gene product of the thermolabile large tumor antigen from the SV40 thermosensitive A58 strain is functional at 33°C but is rapidly degraded at 39.5°C (17, 18). Thus, immortomouse macrophages could be cultured at 33°C, where they proliferate as an immortalized cell line, but fail to proliferate after incubation at 39.5°C.

Animal studies

All animal work was done in accordance with protocols approved by the Institutional Animal Care and Use Committee at The University of Texas MD Anderson Cancer Center. Female athymic nude mice and immune-competent (C57BL/6) mice were purchased from the Animal Production Area of the National Cancer Institute's Frederick Cancer Research and Development Center (Frederick, MD). Homozygous B6.Cg-Csflr (tmlJwp)/J mice were obtained from The Jackson Laboratory. GFP-labeled FVB.Cg-Tg (CAG-EGFP) B5Nagy/J mice, a kind gift from Dr. Michael Andreeff, served as donors for bone marrow transplants. All animals were cared for in accordance with the guidelines set forth by the Association for Assessment and Accreditation of Laboratory Animal Care International and the U.S. Public Health Service Policy on Humane Care and Use. All animals used were 8 to 12 weeks old at the time of injection.

Statistical analysis

A P value of <0.05 was considered statistically significant. We used the Mann–Whitney U test (nonparametric) to compare unmatched groups of values corresponding to xenograft tumor volumes or luminescence signals and tissue protein expression. Differences in apoptosis were analyzed via an unpaired t test comparing the means of two groups of values. We used a Fisher exact test to compare the incidence of metastasis between treatment groups and controls.

Bone marrow transplant

Recipient C57BL/6 mice received 1,000 cGy of radiation and underwent bone marrow transplantation intravenously within 24 hours. Bone marrow from FVB.Cg-Tg(CAG-EGFP)B5Nagy/J mice was harvested, subjected to fluorescence-activated cell sorting to isolate GFP-high expressing cells, suspended in Hank's balanced salt solution (Gibco), and injected into recipient mice. Recipient mice recuperated for 21 days, and then successful transplantation was confirmed by hematologic profiling, including verification of GFP-labeled bone marrow–derived cells.

In vivo model of ovarian cancer and tissue processing

For all animal experiments, cells were harvested using trypsin–ethylenediaminetetraacetic acid (EDTA), neutralized with FBS-containing media, washed, and resuspended to the appropriate cell number in Hank's balanced salt solution prior to injection. For CSF1R$^{-/-}$ mice, IG10 cells (1.25×10^6) were injected intraperitoneally. IG10 (1×10^6) and OVCAR5 (1×10^6) cells were transduced with lentivirus-encoding luciferase and injected into C57BL/6 mice and nude mice, respectively. Mice were imaged once weekly for luminescent signals using a Xenogen IVIS system (Xenogen Corp.). For macrophage infusion, immortomouse macrophages were harvested using trypsin-EDTA, neutralized with FBS-containing media, washed, and resuspended to the appropriate cell number in Hank's balanced salt solution prior to injection of 50 μL intravenously. For syngeneic mouse models, the B20 antibody was administered intraperitoneally at 5 mg/kg twice per week. For nude mouse models, bevacizumab was given intraperitoneally at 6.25 mg/kg twice per week. Zoledronic acid was given intraperitoneally at 1 mg/kg once per week. At the time of necropsy, the weight, number, and distribution of tumors were recorded. Individuals who performed necropsies were blinded to the treatment group assignments. Tissue specimens were fixed with either formalin or optimal cutting temperature compound (Miles Laboratories) or were snap frozen in liquid nitrogen.

Published OnlineFirst August 29, 2017; DOI: 10.1158/1078-0432.CCR-17-0647

Quantitative real-time PCR

The total RNA from either cell lines or tumor tissue was extracted using a QIAGEN RNeasy kit. With 1 μg of RNA, cDNA was synthesized using a Verso cDNA kit (Thermo Scientific) per the manufacturer's instructions. cDNA was then subjected to amplification by real-time PCR using specific primer sequences (100 ng/μL) as specified in Supplementary Table S1. For real-time reverse transcription PCR, we obtained quantitative values (each sample was normalized on the basis of its 18S content) as previously described (19).

Methylation-specific PCR

MethPrimer software (http://www.urogene.org/methprimer/) was used for the prediction of the CpG islands of the VEGFR-1 and VEGFR-3 promoter regions and for design of methylation-specific primers (Supplementary Table S1). Total DNA was isolated from control, B20-sensitive, and B20-resistant Immortomouse macrophage cells using phenol:chloroform extraction, followed by treatment with bisulfite using a methylation kit (EZ DNA Methylation-Gold; Zymo Research). With the use of real-time PCR as described above, quantification of methylation in B20-resistant and -sensitive samples was performed and compared.

Gene expression microarray

Immortalized murine macrophages were treated with B20 for 2 weeks (sensitive) or 6 weeks (resistant), and then RNA was extracted using the mirVana RNA isolation labeling Kit (Ambion). Five hundred nanograms of total RNA were used for labeling and hybridization on a Murine Wg-6 v2 Beadchip (Illumina) according to the manufacturer's protocol. After the bead chips were scanned with an Illumina BeadArray Reader (Illumina), the microarray data were normalized using the quantile normalization method in the Linear Models for Microarray Data package in the R language environment. The expression level of each gene was transformed into a $\log_2$ base before further analysis.

Reverse phase protein arrays

Immortalized murine macrophages were treated with B20 for 2 weeks (sensitive) or 6 weeks (resistant). Cells were harvested at 80% confluence and lysed in modified radioimmunoprecipitation assay buffer (50 mmol/L Tris, 150 mmol/L NaCl, 1% Triton X-100, 0.5% deoxycholate, 25 μg/mL leupeptin, 10 μg/mL aprotinin, 2 mmol/L EDTA, and 1 mmol/L sodium orthovanadate). Reverse phase protein array (RPPA) analysis was performed at the MD Anderson Cancer Center Functional Proteomics RPPA Core Facility using the methods described at the following web address: http://www.mdanderson.org/education-and-research/resources-for-professionals/scientific-resources/core-facilities-and-services/functional-proteomics-rppa-core/index.html. Samples were probed with 161 antibodies by a catalyzed signal amplification approach and visualized by 3,3′-diaminobenzidine chromogen colorimetric reaction. Slides were scanned on a flatbed scanner to produce a 16-bit TIFF image. Spots from TIFF images were identified, and the density was quantified by MicroVigene (VigeneTech). Relative protein levels for each sample were determined by interpolation of each dilution's curves from the "standard curve" (supercurve) of the slide (antibody). All data presented are in fold change compared with the baseline (control treatment). Positive fold change was calculated by dividing each linear value (>1.0) with the average control linear value for each antibody tested, whereas negative fold change (for linear values < 1.0) was also calculated (using the following formula: −1/linear fold change) as in log 2.0 value.

Cytokine assay

Supernatants from cultured ovarian cancer cells were stored at −20°C for batch analyses to measure cytokines. Supernatants were evaluated for cytokines/chemokines using the MILLIPLEX MAP murine cytokine/chemokine panel (Millipore). Cytokine levels were measured in 50 μL of supernatant by Multiplex cytometric bead array (Multiplex) assay on a Luminex 100 analyzer (Luminex Corporation). The intervariability for all inflammatory cytokines tested was less than 10%, indicating the high reliability of the Multiplex-Luminex method of cytokine assay.

Migration and invasion assays

Modified Boyden chambers (Coster) were coated with 0.1% gelatin (for migration assays) or extracellular matrix components (for invasion assays). Untreated, B20-sensitive, and B20-resistant immortomouse macrophages were suspended in 100 μL of serum-free media following 1 hour of exposure to B20 and then added to the upper chamber. Complete media for cells containing 10% FBS (500 μL) were added to the bottom chamber as a chemoattractant. The chambers were incubated at 37°C in 5% CO_2 for 6 hours (migration) or overnight (invasion). After incubation, cells were fixed, stained, and counted in five random fields using light microscopy at ×200.

Cell viability assay

Immortalized murine macrophages sensitive or resistant to anti-VEGF therapy (1×10^4 in 100 μL) were plated in a 96-well plate. After 24 hours, MTT was added to each well. The plate was incubated at 37°C for 20 minutes, and then absorbance was read at 570 nm (CERES UV 900C; Bio-Tek Instruments, Inc.).

Immunostaining

All staining was performed in formalin-fixed, paraffin-embedded 8-μm-thick tumor sections or optimal cutting temperature compound–embedded frozen tissue sections. Following deparaffinization, rehydration, and antigen retrieval or fixation, 3% H_2O_2 was used to block endogenous peroxidase activity for 10 minutes. Protein blocking of nonspecific epitopes was done using either 5% normal horse serum, 1% normal goat serum, or 4% fish gelatin in either PBS or TBS-T (Tris-buffered saline with Tween) for 20 minutes. Slides were incubated with primary antibody for CD68 (Santa Cruz Biotechnology; 1:400), VEGFR-1 (Santa Cruz Biotechnology; 1:500), VEGFR-3 (Millipore; 1:300), E-cadherin (BD Transduction Laboratories; 1:50), vimentin (Cell Signaling Technology; 1:50), cytokeratin wide (Dako; 1:100), or CD31 (BD Pharmingen; 1:800 for mouse tissue) overnight at 4°C. For immunohistochemistry, after the primary antibody was washed with PBS, the appropriate amount of horseradish peroxidase–conjugated secondary antibody was added and visualized with 3,3′-diaminobenzidine chromogen, and counterstaining was done with Gill's Hematoxylin #3. For immunofluorescence, secondary antibody staining was performed with Alexa Fluor 594 or 488 (Molecular Probes). Nuclear staining was performed with Hoechst 33342 (Molecular Probes; #H3570;

Published OnlineFirst August 29, 2017; DOI: 10.1158/1078-0432.CCR-17-0647

1:10,000). Light field images were obtained using a Nikon Microphot-FXA microscope and a Leica DFC320 digital camera (Leica Camera), and immunofluorescent images were obtained using a Zeiss Axioplan 2 microscope and a Hamamatsu ORCA-ER digital camera. To quantify microvessel density, we examined 5 to 10 random fields at ×100 magnification for each tumor (five tumors per group) and counted the microvessels within those fields as previously described (20). A vessel was defined as an open lumen with at least one adjacent CD31-positive cell. Multiple positive cells beside a single lumen were counted as one vessel. Quantification was performed by two investigators in a blinded fashion. Proliferation indices were determined using CellProfiler 2.0 from three representative fields at ×200 magnification for each tumor (five tumors per group). Ki-67–positive cells per high-power field were counted.

Patient tumor samples

Costaining of CD68/VEGFR-1 or of CD68/VEGFR-3 was carried out on paraffin sections obtained from 10 patients with stage III or IV ovarian cancer. The study was approved by the MD Anderson Institutional Review Board. Eighty percent (8/10) of the cases had high-grade serous ovarian cancer, and the remaining had low-grade serous cancer. All patients were treated with bevacizumab plus chemotherapy and were then grouped into responders (complete or partial response) and nonresponders (stable or progressive disease) based on the RECIST guidelines version 1.1.

Results

Macrophage levels increase with the emergence of anti-VEGF therapy resistance

To evaluate the potential role of immune cells in the development of resistance to VEGF blockade, we first established a syngeneic mouse model of adaptive resistance to anti-VEGF therapy. After intraperitoneal injection of luciferase-labeled IG10 murine ovarian cancer cells and after confirmation of tumor establishment with bioluminescence imaging, immunecompetent C57BL/6 mice were randomized to receive (1) control (placebo) or (2) B20 (murine VEGF-A–targeted monoclonal antibody; Genentech Inc.) treatment twice weekly. Both groups underwent weekly bioluminescence imaging to monitor tumor growth. Mice receiving B20 were divided into B20-sensitive and B20-resistant groups, approximately 2 weeks after the start of treatment on the basis of imaging: B20-resistant mice were defined as those with increased tumor growth on treatment, and B20-sensitive mice were defined as responders to the treatment (Fig. 1A and B). All mice were subsequently sacrificed and their tumors collected and analyzed. Compared with the B20-sensitive group, B20-resistant mice had significantly higher tumor burden than controls (Fig. 1C and D; Supplementary Fig. S1A).

Immune profiling was carried out on tumors collected from control, B20-sensitive, and B20-resistant mice using FACS analysis. Compared with B20-sensitive mice, macrophage levels were substantially increased in the tumors of B20-resistant mice, whereas other immune cell populations remained largely unchanged (Fig. 1E and F). $CD68^+$ staining of tumor samples confirmed the increase in macrophage numbers (Fig. 1G and H). In addition, tumors from B20-resistant mice showed higher vessel density than either control or B20-sensitive tumors, as measured by CD31 staining (Fig. 1I and J). The marked increase in macrophages seen along with increased blood vessel density in B20-resistant tumors led us to consider macrophages as potential catalysts in resistance to anti-VEGF therapy.

Depletion of macrophages at the emergence of anti-VEGF resistance restores sensitivity

We next asked whether depletion of macrophages could restore sensitivity to anti-VEGF therapy. Bisphosphonates, such as zoledronic acid and clodronate, are clinically approved for the treatment of osteoporosis and bony metastases, but also induce robust macrophage depletion (21–23). Therefore, we first studied the role of zoledronic acid in anti-VEGF therapy resistance in C57BL/6 mice bearing IG10 tumors. After bioluminescence imaging to confirm the establishment of tumors, mice were randomized to receive (1) control, (2) B20 only, or (3) B20 plus zoledronic acid. The control group received placebo until becoming moribund and these mice were then sacrificed. The B20-only group received treatment twice weekly until the emergence of resistance, defined by an increase in previously stable disease burden on bioluminescence imaging, and were sacrificed when they became moribund. The B20 plus zoledronic acid group received B20 alone until resistance developed; then, weekly zoledronic acid was added to the B20 regimen. The combined treatment was continued until mice became moribund and were sacrificed.

Next, we repeated the above experiment in a different mouse model. In this model, nude mice were injected with luciferase-labeled OVCAR5 (human ovarian cancer cells) and randomized to receive (1) control, (2) bevacizumab only, or (3) bevacizumab plus zoledronic acid. Mice were treated as shown in Fig. 1K. In both experiments, the addition of zoledronic acid at the emergence of resistance halted tumor growth and significantly prolonged survival compared with control or anti-VEGF therapy–only groups (Fig. 1L and M). Also, immunohistochemical staining of tumor samples demonstrated significantly lower macrophage levels in mice receiving B20 plus zoledronic acid (Fig. 1N; Supplementary Fig. S1C) or bevacizumab plus zoledronic acid (Supplementary Fig. S1D and S1E) than in control or anti-VEGF therapy–only groups.

Macrophage-deficient mice have delayed resistance to anti-VEGF therapy

We next examined the contribution of macrophages to anti-VEGF therapy resistance using a murine CSF1R knockout model. $Csf1r^{fl/fl}$ floxed mutant mice possess *loxP* sites flanking exon 5 of the colony-stimulating factor 1 receptor (*Csf1r*) gene (B6.Cg-Csflr (tmlJwp)/J). $CSF1R^{-/-}$ mice were injected intraperitoneally with IG10 cells and randomly assigned to receive (1) control or (2) B20. As additional controls, matched groups of wild-type C57BL/6 mice were injected with IG10 cells and given either no treatment or B20. Treatments began 21 days after cell inoculation, with B20 given twice weekly. Compared with wild-type mice, $CSF1R^{-/-}$ mice receiving no treatment had shorter survival, whereas $CSF1R^{-/-}$ mice receiving B20 failed to develop resistance to VEGF blockade, as illustrated by their prolonged survival and smaller tumor burden (Fig. 2A and B). Immunohistochemical staining confirmed significantly reduced macrophage numbers in $CSF1R^{-/-}$ groups treated with B20 compared with WT and $CSF1R^{-/-}$ control groups (Fig. 2C).

Published OnlineFirst August 29, 2017; DOI: 10.1158/1078-0432.CCR-17-0647

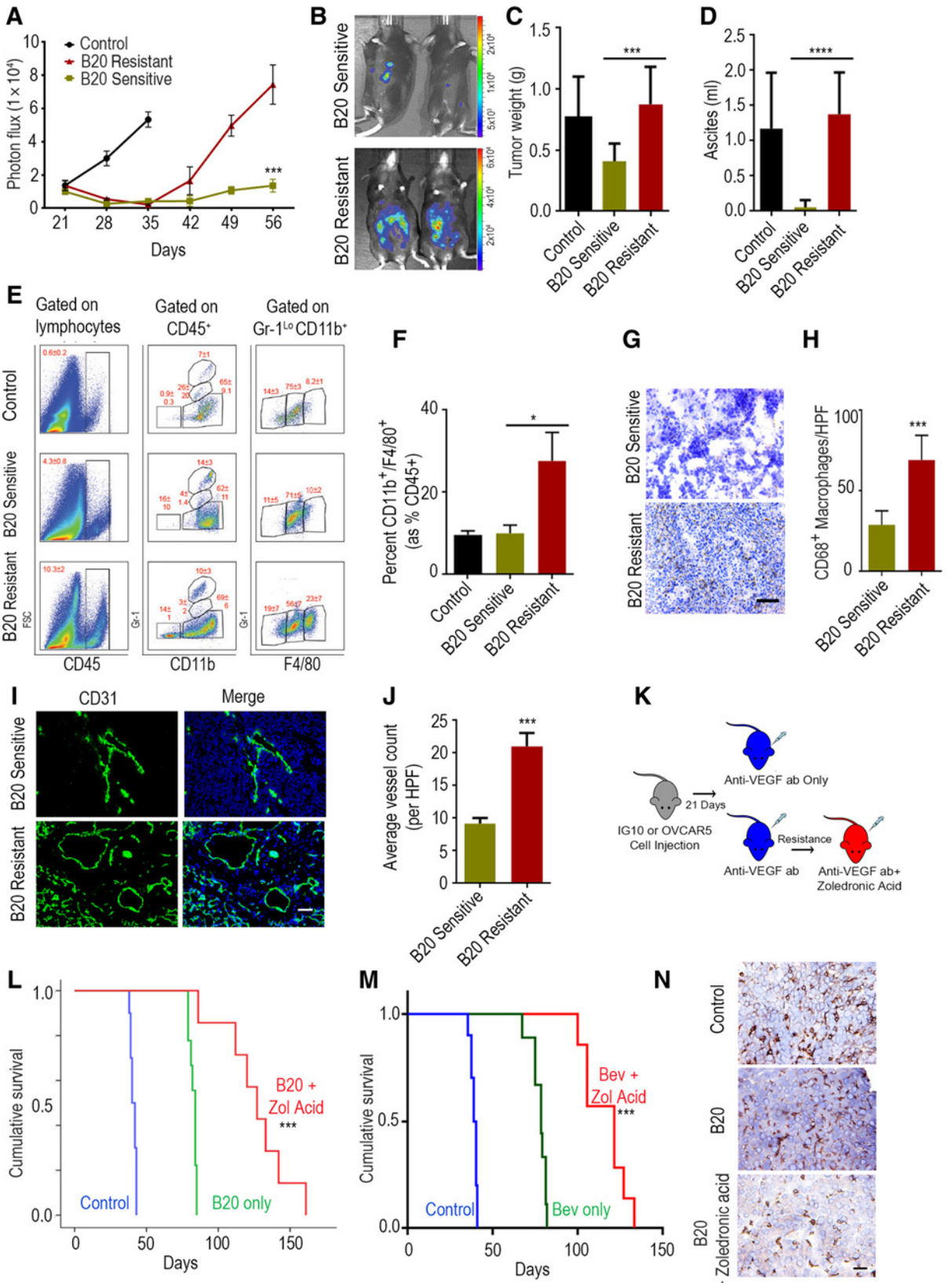

Published OnlineFirst August 29, 2017; DOI: 10.1158/1078-0432.CCR-17-0647

Adding macrophages to macrophage-deficient mice induces anti-VEGF therapy resistance

Next, we investigated whether introduction of macrophages into our CSF1R$^{-/-}$ model would restore the wild-type pattern of anti-VEGF therapy resistance. CSF1R$^{-/-}$ mice were injected with IG10 cells and assigned to receive (1) B20 alone or (2) B20 plus macrophage transfusion. As controls, matched groups of wild-type C57BL/6 mice were also injected with IG10 cells and treated with B20 alone or B20 plus macrophages. Treatments and macrophage infusion began 21 days after cell inoculation to allow for established disease; B20 treatment was given twice weekly. For macrophage infusion, macrophages (5×10^5) were injected intravenously once weekly until they become moribund. Consistent with our results noted above, the survival of CSF1R$^{-/-}$ mice receiving macrophage infusion with B20 recapitulated that of the untreated wild-type mice (Fig. 2D). CSF1R$^{-/-}$ mice treated with B20 alone again failed to develop resistance, whereas all wild-type mice receiving B20 developed resistance following an initial period of sensitivity (Fig. 2D and E). Compared with CSF1R$^{-/-}$ mice treated with B20 alone, CSF1R$^{-/-}$ mice receiving macrophage infusions had tumors with significantly increased macrophage infiltration on immunohistochemical and FACS analyses (Fig. 2F; Supplementary Fig. S2A).

Macrophages with resistance to anti-VEGF therapy are recruited to the tumor microenvironment

Considering the substantial increase in tumor-associated macrophages at the emergence of resistance, as well as recent data suggesting that both resident macrophages and bone marrow–derived macrophages can proliferate (24), we next considered the origin of macrophages that become enriched in the tumor microenvironment with adaptive resistance. Specifically, we investigated whether the increase in macrophages seen at the emergence of resistance was secondary to resident macrophage proliferation or to increased recruitment from bone marrow populations. Bone marrow was isolated from GFP-labeled FVB.Cg-Tg(CAG-EGFP)B5Nagy/J mice (bone marrow donor mice). These mice express GFP in all tissues, including the bone marrow and its derived cells. Following cell sorting to isolate GFP-high expressing cells, the sorted bone marrow donor cells were injected into irradiated (to deplete existing bone marrow) wild-type C57BL/6 recipient mice ($n = 15$). Successful bone marrow transplantation was confirmed by hematologic profiling 3 weeks after transplant, including verification of GFP expression in bone marrow–derived cells (Fig. 2G). Mice were then injected with luciferase-labeled IG10 cells 4 weeks after transplant. Bioluminescence imaging confirmed tumor establishment 21 days after injection of IG10 cells. Three mice were sacrificed, and their tumors harvested to establish baseline characteristics of tumor macrophages. The remaining mice ($n = 12$) received B20 treatment twice weekly and had weekly bioluminescence imaging. Three of these mice were sacrificed and their tumors harvested while they still showed sensitivity to anti-VEGF therapy, as demonstrated by imaging. B20 treatment continued in the remaining mice until resistance to therapy emerged. The mice were then sacrificed, and their tumors were harvested.

In the harvested tumors, macrophages were assessed by immunofluorescence. Bone marrow–derived macrophages were identified by dual expression of GFP and F4/80. In contrast, the resident tissue macrophages were not affected by bone marrow transplant and therefore expressed only F4/80, not GFP. We found that >90% macrophages in resistant tumors were bone marrow derived (Fig. 2H). We also assessed VEGFR-1 expression in the macrophages recruited to the tumor microenvironment with adaptive resistance to anti-VEGF antibody (AVA). Most of the VEGFR-1–negative macrophages were recruited from the bone marrow (Supplementary Fig. S2B).

Macrophage depletion increases the effectiveness of anti-VEGF therapy

In light of our data implicating macrophages in the development of resistance to VEGF blockade, we examined the upfront combination of macrophage depletion with AVA. To investigate resistance to bevacizumab, nude mice were injected with either SKOV3ip1 or OVCAR5 (human ovarian cancer cell lines) and then randomly assigned to receive (1) no treatment, (2) bevacizumab only, (3) zoledronic acid only, or (4) bevacizumab plus zoledronic acid. The mice were sacrificed and their tumors harvested when the mice in any group became moribund. The group treated with bevacizumab plus zoledronic acid had significantly reduced tumor weight and fewer nodules in both the SKOV3ip1 (Fig. 3A) and OVCAR5 (Fig. 3B) models compared with the other groups. We tested these results for consistency using a second bisphosphonate, clodronate, in the SKOV3ip1 model (Supplementary Fig. S3A and S3B). The combination groups using bevacizumab plus either zoledronic acid (Fig. 3C and D) or clodronate (Supplementary Fig. S3C

Figure 1.

Macrophage levels increase with the emergence of anti-VEGF therapy resistance. **A,** C57BL/6 mice that received intraperitoneal injections of IG10 murine ovarian cancer cells were randomly assigned to one of two groups (control or B20 treatment). The control group received placebo until becoming moribund and were then sacrificed. The B20-only group received treatment twice weekly until the emergence of resistance, defined by an increase in previously stable disease burden on bioluminescence imaging, and were sacrificed when they became moribund. Bioluminescence imaging was performed once weekly. The color scale bars depicting the photon fluxes emitted from the tumor cells are shown. **B,** Quantitative representation of bioluminescence. **C,** Bar graph shows the average tumor weight **(D)** and ascites. **E,** Immune profiling of tumors from B20-sensitive and -resistant tumors. **F,** Quantitative representation of CD11b$^+$/F4/80$^+$ macrophages. **G,** Representative immunohistochemical images of B20-sensitive and -resistant tumors with CD68 expression. Scale bars, 100 μm. **H,** Quantitative representation of macrophage levels in B20-sensitive and -resistant tumors. **I,** CD31 antibody staining of sections of the B20-sensitive and -resistant tumors. Scale bars, 100 μm. **J,** Quantitative representations of blood vessel count in both groups. **K,** Schematic representation of the experimental setup. **L,** The impact of B20 and zoledronic acid treatment on survival in mice. Mice bearing IG10 tumors were treated with control, B20, or B20 plus zoledronic acid (Zol). A Kaplan–Meier curve was used to analyze the survival difference between control and treatment groups ($n = 10$). **M,** The above experiment was repeated using human ovarian cancer line OVCAR5. A Kaplan–Meier curve was used to analyze the survival difference between control and treatment groups ($n = 10$). **N,** Representative immunohistochemical images of IG10 tumor sections following control, B20, or B20 plus zoledronic acid treatment. The sections were stained using CD68 antibody. Scale bars, 100 μm. Mean ± SEM values are shown. ***, $P < 0.001$ and ****, $P < 0.0001$.

Published OnlineFirst August 29, 2017; DOI: 10.1158/1078-0432.CCR-17-0647

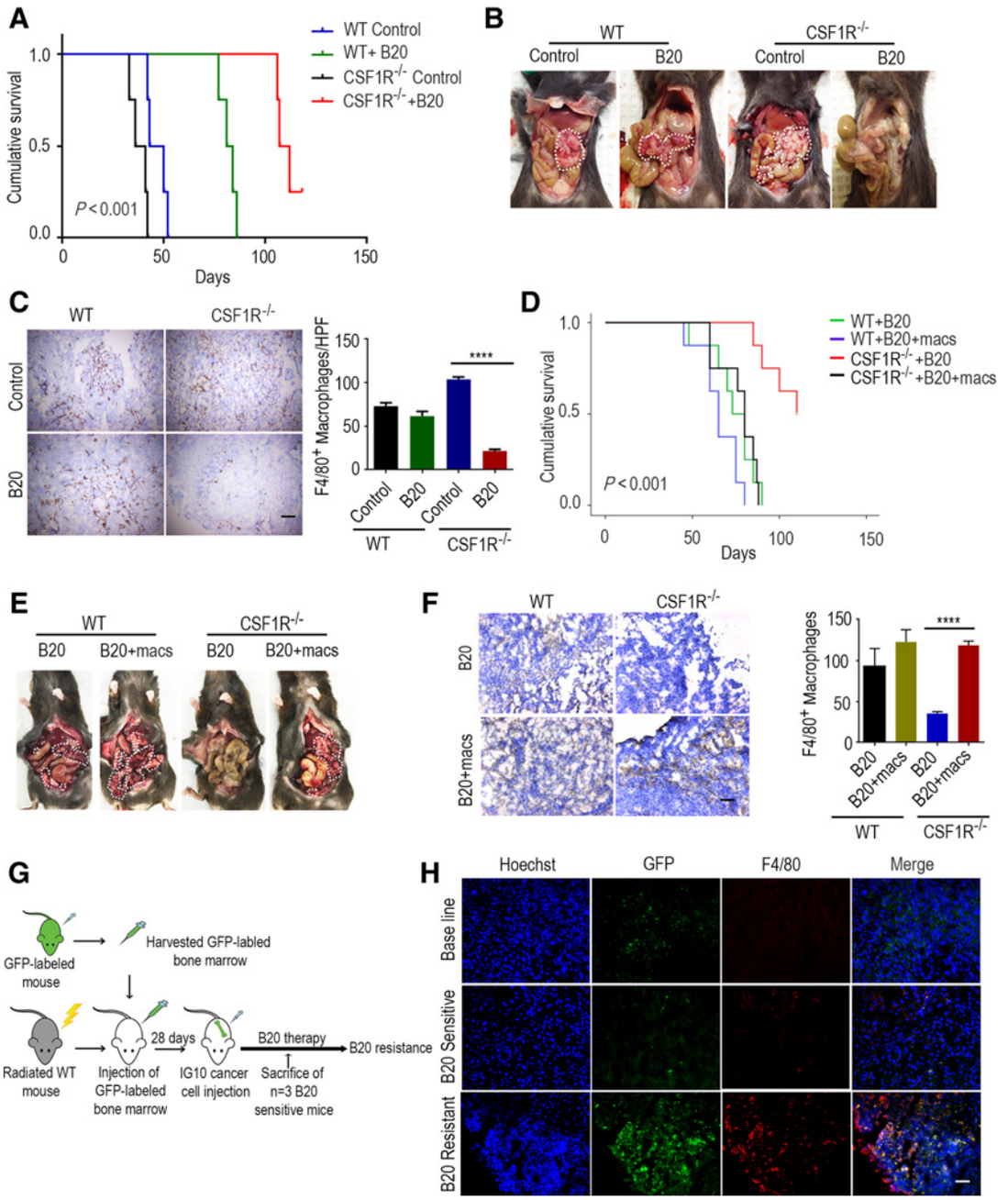

Figure 2.

Macrophage-deficient mice do not develop resistance to anti-VEGF therapy. **A,** WT and CSF1R$^{-/-}$ mice were injected intraperitoneally with IG10 cells. These mice were assigned to 4 groups (10 mice/group): group 1 WT mice treated with control antibody, group 2 was WT mice received the B20 antibody, group 3 was CSF1R$^{-/-}$ mice administered control antibody, and group 4 was CSF1R$^{-/-}$ mice treated with the B20 antibody. A Kaplan–Meier curve was used to analyze the survival difference between control and treatment groups. **B,** Representative images of the extent of metastatic spread in both WT and CSF1R$^{-/-}$ mice following control vs. B20 treatment. Metastatic areas are outlined with dotted white lines. **C,** Immunohistochemical staining using CD68 antibody on control or B20-treated tumor sections from WT and CSF1R$^{-/-}$ mice. Scale bars, 100 μm. Bar graph represents the quantification of macrophage expression. **D,** WT and CSF1R$^{-/-}$ mice were injected intraperitoneally with IG10 cells and were assigned to 4 groups (10 mice/group): groups 1 and 2 were WT mice treated with either B20 alone or with injection of B20^{+} macrophages. Groups 3 and 4 were CSF1R$^{-/-}$ mice following B20 alone or with injection of B20^{+} macrophages. A Kaplan–Meier curve was used to analyze the survival difference between control and treatment groups. **E,** Representative images of the extent of metastatic spread in both WT and CSF1R$^{-/-}$ mice following B20 treatment with or without macrophage injection. Metastatic areas are outlined with dotted white lines. **F,** Immunohistochemical staining using CD68 antibody following B20 treatment with or without macrophage injected tumor sections from both WT and CSF1R$^{-/-}$ mice. Scale bars, 100 μm. Bar graph represents the quantification of macrophage expression. **G,** Schematic representation of experimental setup. **H,** Bone marrow was isolated from GFP-labeled FVB. Cg-Tg(CAG-EGFP)B5Nagy/J donor mice and injected into irradiated WT recipient mice following B20 treatment. Representative images of immunofluorescence staining of F4/80 and GFP on B20-sensitive and -resistant tumor sections. Scale bars, 100 μm. Mean ± SEM values are shown. ****, $P < 0.0001$.

Published OnlineFirst August 29, 2017; DOI: 10.1158/1078-0432.CCR-17-0647

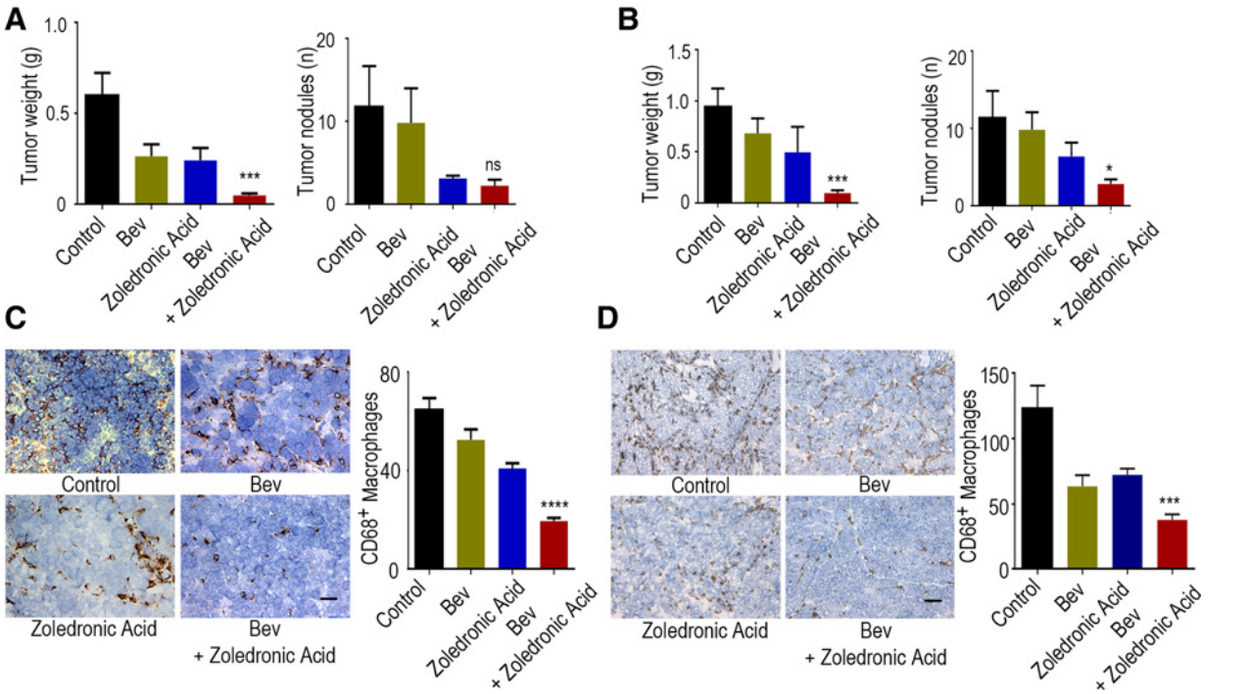

Figure 3.

Macrophage depletion increases the effectiveness of anti-VEGF therapy. **A,** Nude mice were injected with SKOV3ip1 tumor cells into the peritoneal cavity followed by bevacizumab and zoledronic acid treatment. At the end of the study, mice were euthanized, tumors were harvested, and average tumor weight and number of nodules is shown. **B,** Aggregate mass of intraperitoneal implanted OVCAR5 tumor and number of nodules followed by bevacizumab and zoledronic acid treatment. **C,** Immunohistochemical staining using CD68 antibody on bevacizumab and zoledronic acid treated on SKOV3ip1 tumor sections. Scale bars, 100 μm. Bar graph represents the quantification of $CD68^+$ staining. **D,** Representative images and quantification of CD68 staining on OVCAR5-induced tumor followed by bevacizumab and zoledronic acid treatment. Mean ± SEM values are shown. Control vs. combination *, $P < 0.05$; ***, $P < 0.001$; and ****, $P < 0.0001$.

and S3D) demonstrated significantly fewer macrophages than the other groups did. This decrease in macrophage infiltration in the combination groups mirrors the results seen in anti-VEGF therapy–sensitive tumors in our initial immune profiling (Fig. 1E and F; Supplementary Fig. S1B). We also checked for polarization status of infiltrating macrophages in the group of mice showing anti-VEGF resistance. We found that infiltrating macrophages in resistant groups were positive for CXCL 9 and CXCL 10 (M1 macrophage chemokine receptors), whereas there was no colocalization with F4/80 and MR (mannose receptor; marker for M2 macrophage population) expression (Supplementary Fig. S3E).

Anti-VEGF therapy–resistant macrophages have heightened viability, migration, and invasion

To identify potential differences between AVA-sensitive and -resistant macrophages that might contribute to resistance, we compared the cell viability of these macrophages using a 3-(4,5-dimethylthiazol-2-yl)-2,5-diphenyltetrazolium bromide (MTT) assay. After exposure to either 2 weeks (to reflect the anti-VEGF therapy–sensitive condition) or 6 weeks (to reflect the AVA-resistant condition) of B20 treatment, murine macrophages were exposed to MTT, and cell viability was assessed. Compared with sensitive macrophages, resistant macrophages demonstrated a 73% increase in cell viability (Supplementary Fig. S4A). In addition, we assessed apoptosis in AVA-sensitive and -resistant macrophages. Resistant macrophages displayed significantly increased resistance to apoptosis following exposure to paclitaxel (Supplementary Fig. S4B).

On the basis of the increased recruitment of macrophages at the emergence of resistance, we investigated differences in the ability of AVA-sensitive and -resistant macrophages to invade and migrate following exposure to an anti-VEGF drug. Both groups of macrophages were exposed to B20 for 1 hour and then plated into modified Boyden chambers. Migration and invasion were subsequently assessed at 6 and 24 hours, respectively. As predicted, sensitive macrophages displayed significantly inhibited migration and invasion following exposure to B20. In contrast, the ability of resistant macrophages to migrate and invade was not affected by exposure to B20 (Supplementary Fig. S4C and S4D).

Anti-VEGF therapy–resistant macrophages express low VEGFR and secrete alternative proangiogenic cytokines

To assess phenotypic differences between AVA-sensitive and -resistant macrophages, we performed a cytokine array. Supernatant was collected from murine macrophages exposed to either 2 weeks (sensitive) or 6 weeks (resistant) of B20 treatment and evaluated for cytokines/chemokines using the MILLIPLEX MAP murine cytokine/chemokine panel (Millipore). Compared with sensitive macrophages, resistant

Published OnlineFirst August 29, 2017; DOI: 10.1158/1078-0432.CCR-17-0647

macrophages secreted significantly less VEGF and instead showed increased secretion of alternative proangiogenic cytokines and chemokines, including PDGF and G-CSF (Fig. 4A).

Concurrently, we compared macrophage populations in the sensitive and resistant conditions using RPPA. Immortalized murine macrophages were harvested and protein extracted

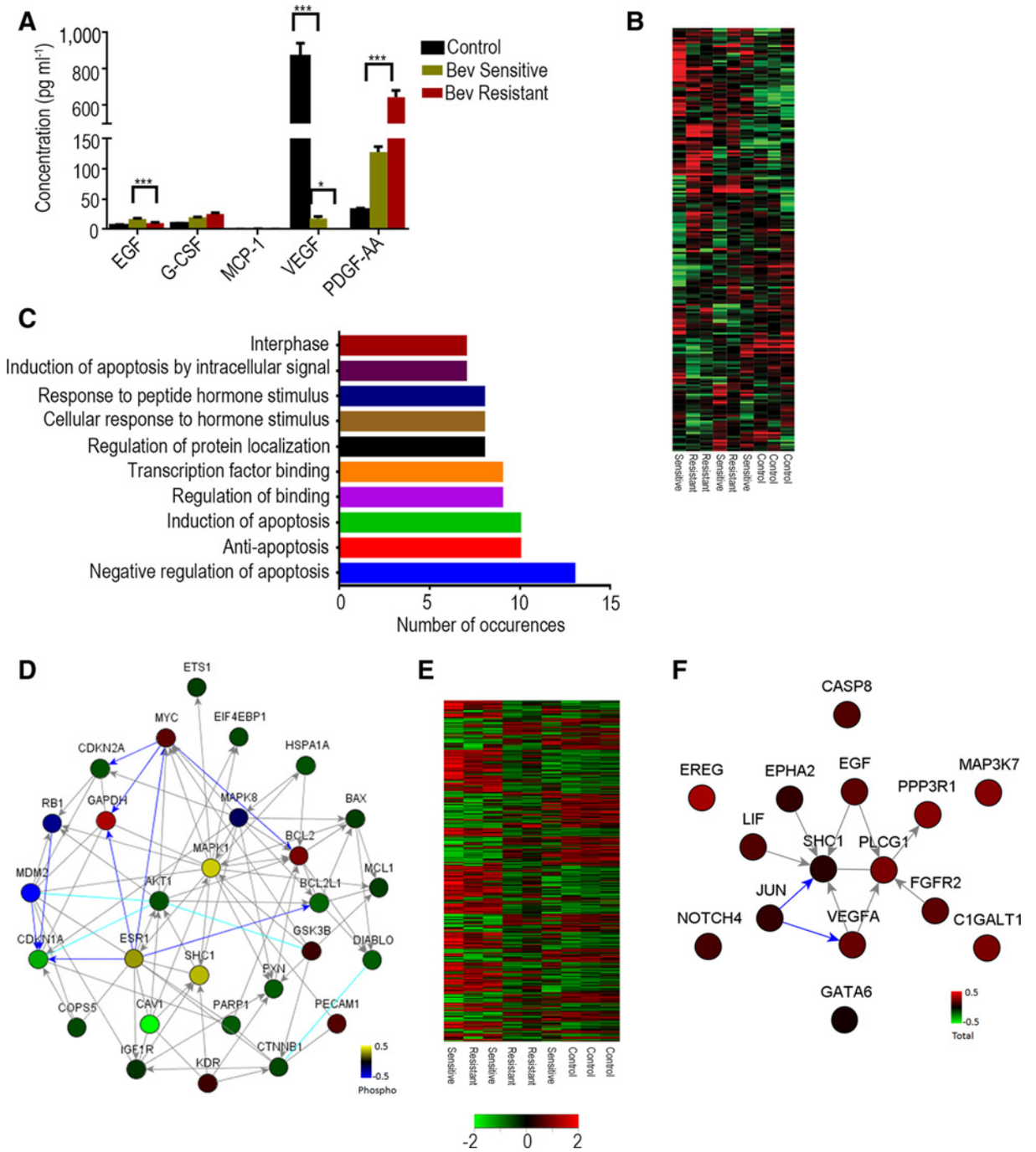

Figure 4.

Anti-VEGF therapy–resistant macrophages express alternate proangiogenic cytokines. **A,** Cytokine array using supernatant from bevacizumab (Bev) sensitive and resistant macrophages. **B,** Heat map represents normalized protein expression levels obtained from the RPPA array using sensitive and resistant macrophages. **C,** Pathway analysis of RPPA array. **D,** Netwalker analysis of RPPA data between sensitive and resistant macrophages. **E,** Heat map represents normalized gene expression levels obtained from the mRNA array between sensitive and resistant macrophages. **F,** Netwalker analysis of gene expression between sensitive and resistant macrophages. Mean ± SEM values are shown. *, $P < 0.05$ and ***, $P < 0.001$.

Published OnlineFirst August 29, 2017; DOI: 10.1158/1078-0432.CCR-17-0647

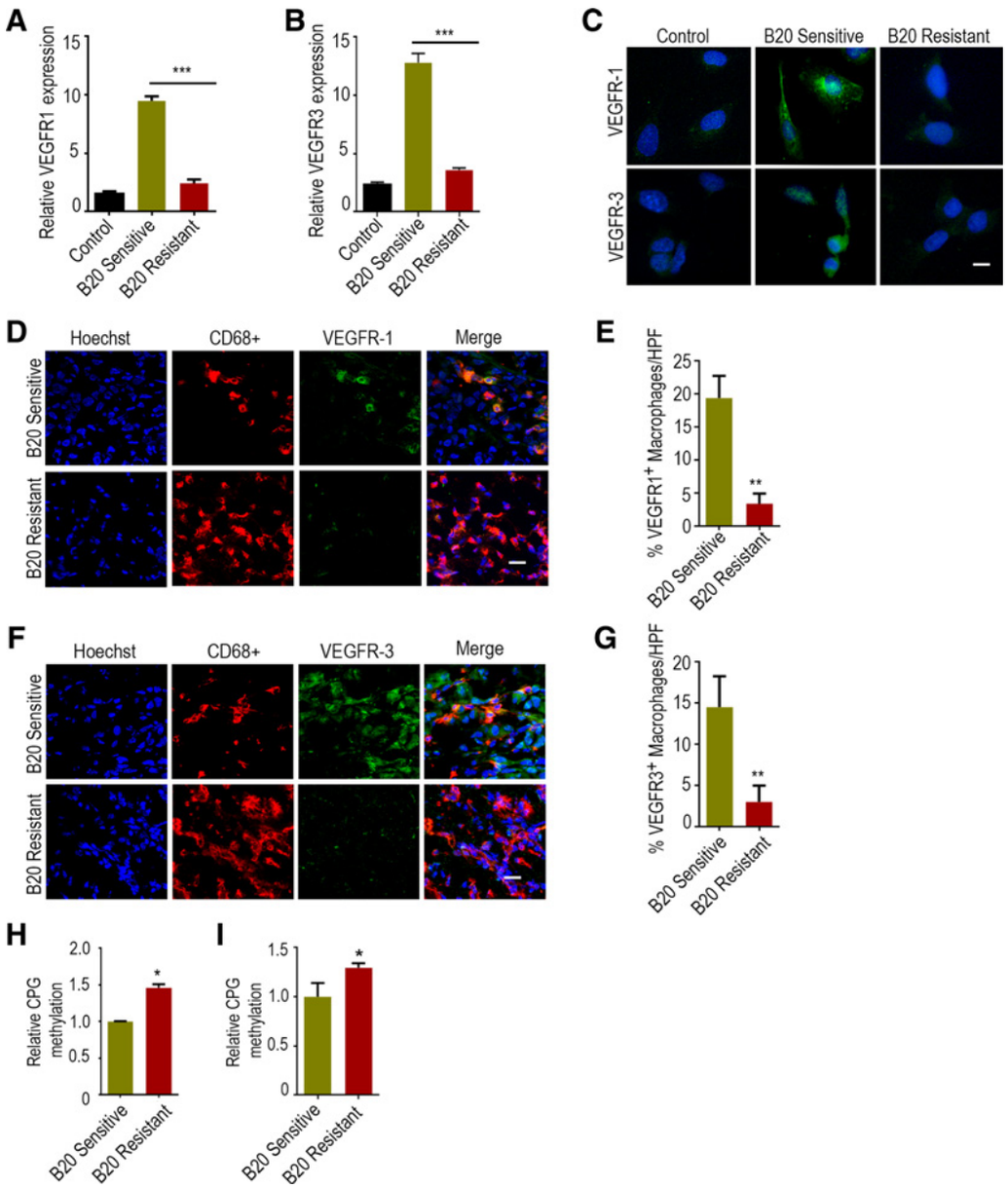

Figure 5.

Anti-VEGFR expression on macrophages correlates with clinical outcome of anti-VEGF therapy, and anti-VEGF therapy–resistant macrophages shows methylation on VEGFR promoters. Downregulation of VEGFR-1 **(A)** and VEGFR-3 **(B)** mRNA in the setting of anti-VEGF therapy resistance. **C,** Immunofluorescence staining of macrophage VEGFR-1 and VEGFR-3 expression following treatment with B20 in sensitive and resistant macrophages. Scale bars, 20 μm. Representative images of macrophage expression of **(D)** VEGFR-1 in B20-sensitive and B20-resistant tumors. **E,** Bar graph represents the percentage of VEGFR-1–expressing macrophages in B20-sensitive and -resistant tumors. **F,** Representative images of VEGFR-3–expressing macrophages in B20-sensitive and -resistant tumors. Scale bars, 100 μm. **G,** Percentage of VEGFR-3–expressing macrophages in B20-sensitive and -resistant tumors. **H,** VEGFR-1 CPG methylation by methylation-specific polymerase chain reaction (MSP). **I,** VEGFR-3 CPG methylation by MSP. Mean ± SEM values are shown. *, $P < 0.05$; **, $P < 0.01$; and ***, $P < 0.001$.

following 2 weeks (sensitive) or 6 weeks (resistant) of treatment with B20 *in vitro*. Pathway analysis again demonstrated that the VEGFR-interacting network is downregulated in the resistant population (Fig. 4B–D; Supplementary Fig. S4E).

Considering the significant differences in macrophage numbers in the AVA-sensitive and -resistant settings, we investigated the genotypic differences between these populations. Immortalized murine macrophages were cultured *in vitro* and treated with B20 twice weekly. Macrophages were collected at 2 weeks (sensitive) and 6 weeks (resistant), and gene expression profiling was performed on isolated RNA. Analysis of these data revealed significant downregulation of the VEGF pathway and upregulation of

Published OnlineFirst August 29, 2017; DOI: 10.1158/1078-0432.CCR-17-0647

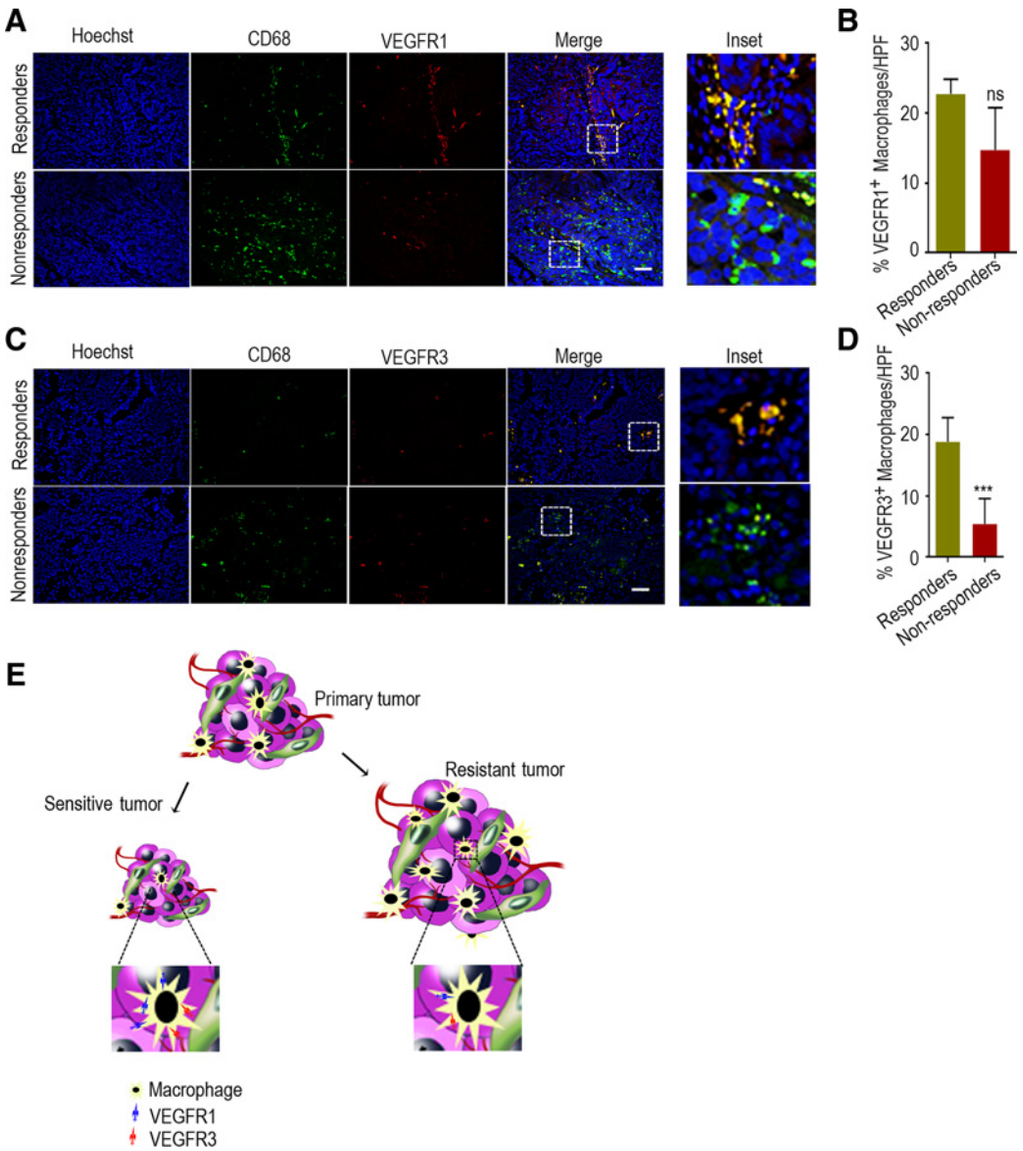

Figure 6

VEGFR expression on macrophages correlates with clinical outcome. **A,** Immunofluorescence staining of macrophages along VEGFR-1 expression following anti-VEGF therapy in patient samples (5 samples/group). **B,** Bar graph represents the VEGFR-1–expressing macrophages. **C,** Immunofluorescence staining of macrophages along VEGFR-3 expression following anti-VEGF therapy in patient samples. **D,** Bar graph represents the VEGFR-1–expressing macrophages. Scale bars, 20 μm. **E,** Schematic representation of a hypothetical model. Mean ± SEM values are shown. ***, $P < 0.001$.

alternative proangiogenic pathways in resistant macrophages compared with sensitive macrophages (Fig. 4E and F).

VEGFR expression is decreased, and VEGFR promoters are methylated in anti-VEGF therapy–resistant macrophages

On the basis of the downregulation of VEGF receptors seen in the gene expression profiling of resistant macrophages, we assessed VEGFR expression on macrophages *in vitro*. Cultured immortalized murine macrophages were treated with B20 twice weekly. VEGFR expression was assessed by qPCR at baseline as a control, 2 weeks (sensitive), and 6 weeks (resistant). We found that following an initial period of upregulation during the AVA-sensitive phase, VEGFR-1 and VEGFR-3 expressions were significantly downregulated in the setting of anti-VEGF therapy resistance at both RNA (Fig. 5A and B) and VEGFR-1 protein expression (Supplementary Fig. S5A). These results were confirmed by immunofluorescence staining (Fig. 5C). In parallel, we assessed colocalization of CD68, a macrophage marker, and of VEGFR-1 and VEGFR-3 from *in vivo* AVA-sensitive and -resistant tumor samples. Again, we noted less macrophage expression of VEGFR-1 (Fig. 5D and E) and VEGFR-3 (Fig. 5F and G) in resistant tumors than in sensitive tumors.

Published OnlineFirst August 29, 2017; DOI: 10.1158/1078-0432.CCR-17-0647

We next sought to uncover the mechanism of macrophage VEGFR-1 and VEGFR-3 downregulation. We investigated changes in transcription, translation, and protein stability between sensitive and resistant states and found that transcription alterations predominated. To further explore the mechanisms responsible for these changes, we assessed methylation of the promoter regions of VEGFR-1 and VEGFR-3. DNA samples from AVA-sensitive and -resistant immortalized murine macrophages were treated with bisulfite, and methylation-specific polymerase chain reaction (MSP) analysis was performed, revealing a significant increase in methylation at the VEGFR-1 and VEGFR-3 promoter regions in resistant macrophages (Fig. 5H and I).

To test the biological consequences of macrophages based on VEGFR expression, we treated established SKOV3ip1 tumors with VEGFR-1–positive or –negative macrophages along with AVA and evaluated tumor burden. Tumors injected with VEGFR-1–positive macrophages responded to AVA, whereas those injected with VEGFR-1–negative macrophages continued to grow (Supplementary Fig. S5B).

VEGFR expression on macrophages correlates with clinical outcome of anti-VEGF therapy

Next, we investigated the role of macrophage VEGFR expression on anti-VEGF therapy–resistant ovarian cancer in patients. Using patient data, we assessed pretreatment macrophage VEGFR expression as a possible predictor of response to anti-VEGF therapy. Paraffin sections from pretreatment ovarian cancer biopsy specimens (5 samples in each case) were stained for CD68 and VEGFR expression. Macrophage VEGFR expression was then correlated with clinical response to anti-VEGF therapy. We observed a trend of low macrophage VEGFR expression in nonresponders against anti-VEGF therapy (Fig. 6A–D). Figure 6E shows a schematic representation of the model to reflect the findings from this article.

Discussion

In the current study, we demonstrate a previously unrecognized role of macrophages in resistance to VEGF blockade. These macrophages are actively recruited to the tumor microenvironment from the bone marrow, where their accumulation correlates with the emergence of anti-VEGF therapy resistance. The downregulation of VEGFR-1 and VEGFR-3 accompanies upregulation of alternative angiogenic pathways, facilitating escape from VEGF-directed therapies.

Importantly, the depletion of macrophages using bisphosphonates at the emergence of anti-VEGF therapy resistance halted tumor growth and prolonged survival in our murine model. We show that bisphosphonates plus anti-VEGF therapy can prevent the development of resistance and improve the effectiveness of antiangiogenic therapy. These findings offer direct support to previous clinical observations that bisphosphonates reduce bone metastasis in patients with breast cancer and in those with prostate or renal cell carcinoma and pre-existing bone metastasis, resulting in a trend toward increased survival (25, 26). Also, we demonstrate modulation of macrophage VEGFR in response to anti-VEGF therapy, with significant VEGFR downregulation in resistant tumors. This expression of VEGFR is dynamic and reflects changes at the level of the tumor microenvironment in response to VEGF blockade. In patient samples, we show that macrophage VEGFR expression may predict response to antiangiogenic therapy.

Our study has important clinical implications. In light of the role of macrophages in resistance to VEGF blockade, strategies to modify macrophage response should be investigated in combination with anti-VEGF therapy. Possible approaches include bisphosphonates, as described here (e.g., CSF-1 or CCR2 inhibitors, and trabectedin; refs. 27–29). The upfront combination of these therapies with VEGF blockade could be considered for diminishing the opportunity of macrophages to contribute to anti-VEGF therapy resistance. In addition, macrophage VEGFR expression offers potential as a predictor of response to anti-VEGF therapy and may serve as a testable measure of resistance in patients receiving antiangiogenic therapy.

In summary, we reveal a previously unrecognized role of macrophages in resistance to anti-VEGF therapy. Macrophage depletion could be used to improve the effectiveness of VEGF blockade. Macrophage VEGFR expression may be a predictor of response to antiangiogenic therapy. These readily translatable findings warrant further clinical investigation.

Disclosure of Potential Conflicts of Interest

No potential conflicts of interest were disclosed.

Authors' Contributions

Conception and design: H.J. Dalton, S. Pradeep, M. McGuire, J.M. Hansen, V. Gonzalez-Villasana, S.Y. Wu, G. Lopez-Berestein, A.K. Sood

Development of methodology: H.J. Dalton, S. Pradeep, M. McGuire, R.A. Previs, V. Gonzalez-Villasana, S.Y. Wu, M. Bar-Eli, W. Overwijk, A.K. Sood

Acquisition of data (provided animals, acquired and managed patients, provided facilities, etc.): H.J. Dalton, S. MA, Y. Lyons, G.N. Armaiz-Pena, R.A. Previs, J.M. Hansen, R. Rupaimoole, M.S. Cho, S.Y. Wu, L.S. Mangala, R. Langley, H. Mu, A.K. Sood

Analysis and interpretation of data (e.g., statistical analysis, biostatistics, computational analysis): H.J. Dalton, S. Pradeep, M. McGuire, Y. Hailemichael, Y. Lyons, R. Rupaimoole, R. Langley, M. Andreeff, P. Ram, G. Lopez-Berestein, R.L. Coleman

Writing, review, and/or revision of the manuscript: H.J. Dalton, S. Pradeep, Y. Lyons, R.A. Previs, J.M. Hansen, S.Y. Wu, N.B. Jennings, W. Hu, R. Langley, W. Overwijk, P. Ram, G. Lopez-Berestein, R.L. Coleman, A.K. Sood

Administrative, technical, or material support (i.e., reporting or organizing data, constructing databases): H.J. Dalton, S. Pradeep, Y. Lyons, R.A. Previs, J.M. Hansen, S.Y. Wu, N.B. Jennings, W. Hu, W. Overwijk, P. Ram, G. Lopez-Berestein, R.L. Coleman, A.K. Sood

Study supervision: S. Pradeep, A.K. Sood

Grant Support

Portions of this work were supported by the NIH (CA016672, CA109298, P50 CA083639, P50 CA098258, and UH3 TR000943), U01 CA213759 NCI-DHHS-NIH T32 Training grant (T32 CA101642), the V-Foundation, the Ovarian Cancer Research Fund, Inc. (Program Project Development Grant), the Gateway Foundation, the Blanton-Davis Ovarian Cancer Research Program, the Judi Rees Fund, the American Cancer Society Research Professor Award, and the Frank McGraw Memorial Chair in Cancer Research. S. Pradeep is supported by the Foundation for Women's Cancer grant and Liz Tilberis Early Career Award. Y. Lyons is supported by Keck Center of the Gulf Coast Consortia.

The costs of publication of this article were defrayed in part by the payment of page charges. This article must therefore be hereby marked *advertisement* in accordance with 18 U.S.C. Section 1734 solely to indicate this fact.

Received March 9, 2017; revised June 15, 2017; accepted August 22, 2017; published OnlineFirst August 29, 2017.

Published OnlineFirst August 29, 2017; DOI: 10.1158/1078-0432.CCR-17-0647

References

1. Hanahan D, Weinberg RA. The hallmarks of cancer. Cell 2000;100:57–70.
2. Ferrara N.VEGF as a therapeutic target in cancer. Oncology 2005;11–6.
3. Masoumi Moghaddam S, Amini A, Morris DL, Pourgholami MH. Significance of vascular endothelial growth factor in growth and peritoneal dissemination of ovarian cancer. Cancer Metast Rev 2012;31:143–62.
4. Sitohy B, Nagy JA, Dvorak HF. Anti-VEGF/VEGFR therapy for cancer: reassessing the target. Cancer Res 2012;72:1909–14.
5. Kerbel RS.Tumor angiogenesis. N Eng J Med 2008;358:2039–49.
6. Fox WD, Higgins B, Maiese KM, Drobnjak M, Cordon-Cardo C, Scher HI, et al. Antibody to vascular endothelial growth factor slows growth of an androgen-independent xenograft model of prostate cancer. Clin Cancer Res 2002;8:3226–31.
7. Mancuso MR, Davis R, Norberg SM, O'Brien S, Sennino B, Nakahara T, et al. Rapid vascular regrowth in tumors after reversal of VEGF inhibition. J Clin Invest 2006;116:2610–21.
8. Burger RA, Brady MF, Bookman MA, Fleming GF, Monk BJ, Huang H, et al. Incorporation of bevacizumab in the primary treatment of ovarian cancer. N Eng J Med 2011;365:2473–83.
9. Perren TJ, Swart AM, Pfisterer J, Ledermann JA, Pujade-Lauraine E, Kristensen G, et al. A phase 3 trial of bevacizumab in ovarian cancer. N Eng J Med 2011;365:2484–96.
10. Burger RA, Sill MW, Monk BJ, Greer BE, Sorosky JI. Phase II trial of bevacizumab in persistent or recurrent epithelial ovarian cancer or primary peritoneal cancer: a Gynecologic Oncology Group Study. J Clin Oncol 2007;25:5165–71.
11. Scavelli C, Nico B, Cirulli T, Ria R, Di Pietro G, Mangieri D, et al. Vasculogenic mimicry by bone marrow macrophages in patients with multiple myeloma. Oncogene 2008;27:663–74.
12. Shojaei F, Wu X, Malik AK, Zhong C, Baldwin ME, Schanz S, et al. Tumor refractoriness to anti-VEGF treatment is mediated by CD11b+Gr1+ myeloid cells. Nat Biotechnol 2007;25:911–20.
13. Dijkgraaf EM, Heusinkveld M, Tummers B, Vogelpoel LT, Goedemans R, Jha V, et al. Chemotherapy alters monocyte differentiation to favor generation of cancer-supporting m2 macrophages in the tumor microenvironment. Cancer Res 2013;73:2480–92.
14. De Palma M, Lewis CE. Macrophage regulation of tumor responses to anticancer therapies. Cancer Cell 2013;23:277–86.
15. Kozin SV, Kamoun WS, Huang Y, Dawson MR, Jain RK, Duda DG. Recruitment of myeloid but not endothelial precursor cells facilitates tumor regrowth after local irradiation. Cancer Res 2010;70:5679–85.
16. Mazzieri R, Pucci F, Moi D, Zonari E, Ranghetti A, Berti A, et al. Targeting the ANG2/TIE2 axis inhibits tumor growth and metastasis by impairing angiogenesis and disabling rebounds of proangiogenic myeloid cells. Cancer Cell 2011;19:512–26.
17. Jat PS, Noble MD, Ataliotis P, Tanaka Y, Yannoutsos N, Larsen L, et al. Direct derivation of conditionally immortal cell lines from an H-2Kb-tsA58 transgenic mouse. Proc Nat Acad Sci U S A 1991;88:5096–100.
18. Minokoshi Y, Kim YB, Peroni OD, Fryer LG, Muller C, Carling D, et al. Leptin stimulates fatty-acid oxidation by activating AMP-activated protein kinase. Nature 2002;415:339–43.
19. Thaker PH, Deavers M, Celestino J, Thornton A, Fletcher MS, Landen CN, et al. EphA2 expression is associated with aggressive features in ovarian carcinoma. Clin Cancer Res 2004;10:5145–50.
20. Landen CN Jr., Chavez-Reyes A, Bucana C, Schmandt R, Deavers MT, Lopez-Berestein G, et al. Therapeutic EphA2 gene targeting in vivo using neutral liposomal small interfering RNA delivery. Cancer Res 2005;65:6910–8.
21. Clezardin P.Bisphosphonates' antitumor activity: an unravelled side of a multifaceted drug class. Bone 2011;48:71–9.
22. Li X, Liao J, Park SI, Koh AJ, Sadler WD, Pienta KJ, et al. Drugs which inhibit osteoclast function suppress tumor growth through calcium reduction in bone. Bone 2011;48:1354–61.
23. Kyle RA, Yee GC, Somerfield MR, Flynn PJ, Halabi S, Jagannath S, et al. American Society of Clinical Oncology 2007 clinical practice guideline update on the role of bisphosphonates in multiple myeloma. J Clin Oncol 2007;25:2464–72.
24. Davies LC, Rosas M, Jenkins SJ, Liao CT, Scurr MJ, Brombacher F, et al. Distinct bone marrow-derived and tissue-resident macrophage lineages proliferate at key stages during inflammation. Nat Commun 2013;4:1886.
25. Wong MH, Stockler MR, Pavlakis N. Bisphosphonates and other bone agents for breast cancer. Cochrane Database Syst Rev 2012;2:CD003474.
26. Coleman R, Gnant M, Morgan G, Clezardin P. Effects of bone-targeted agents on cancer progression and mortality. J Nat Cancer Inst 2012;104:1059–67.
27. DeNardo DG, Brennan DJ, Rexhepaj E, Ruffell B, Shiao SL, Madden SF, et al. Leukocyte complexity predicts breast cancer survival and functionally regulates response to chemotherapy. Cancer Discov 2011;1:54–67.
28. Mitchem JB, Brennan DJ, Knolhoff BL, Belt BA, Zhu Y, Sanford DE, et al. Targeting tumor-infiltrating macrophages decreases tumor-initiating cells, relieves immunosuppression, and improves chemotherapeutic responses. Cancer Res 2013;73:1128–41.
29. Germano G, Frapolli R, Belgiovine C, Anselmo A, Pesce S, Liguori M, et al. Role of macrophage targeting in the antitumor activity of trabectedin. Cancer Cell 2013;23:249–62.

Published OnlineFirst August 29, 2017; DOI: 10.1158/1078-0432.CCR-17-0647

Clinical Cancer Research

Macrophages Facilitate Resistance to Anti-VEGF Therapy by Altered VEGFR Expression

Heather J. Dalton, Sunila Pradeep, Michael McGuire, et al.

Clin Cancer Res 2017;23:7034-7046. Published OnlineFirst August 29, 2017.